Electronic and atomic structure of the $6H$-SiC$(000\bar{1})$ surface studied by ARPES, LEED, and XPS

M. Hollering
Institut für Technische Physik, Universität Erlangen-Nürnberg, D-91058 Erlangen, Germany

J. Bernhardt and J. Schardt
Lehrstuhl für Festkörperphysik, Universität Erlangen-Nürnberg, Staudtstrasse 7, D-91058 Erlangen, Germany

A. Ziegler, R. Graupner, and B. Mattern
Institut für Technische Physik, Universität Erlangen-Nürnberg, D-91058 Erlangen, Germany

A. P. J. Stampfl
Department of Physics, La Trobe University, Victoria 3083, Australia

U. Starke and K. Heinz
Lehrstuhl für Festkörperphysik, Universität Erlangen-Nürnberg, Staudtstrasse 7, D-91058 Erlangen, Germany

L. Ley
Institut für Technische Physik, Universität Erlangen-Nürnberg, D-91058 Erlangen, Germany

(Received 19 February 1998)

We present an investigation of the electronic and geometric structure of the carbon terminated $6H$-SiC(0001) surface. The samples were prepared in different ways that result in the same unreconstructed (1×1) surface. From angle-resolved photoemission spectra taken along the $\bar{\Gamma}\,\bar{M}$ and the $\bar{\Gamma}\,\bar{K}$ azimuth, the strong dispersion of a surface state in the ionic gap and of a bulk state at the boundary of the ionic gap is measured. This indicates unambiguously that large areas of the surface are well ordered. The comparison with band-structure calculations shows that even these areas do not have the properties of an intrinsic $6H$-SiC(0001) surface. From a low-energy electron diffraction (LEED) structure analysis of the same surface a model is determined with domains of all three possible bilayer truncations of the bulk unit cell present at the surface with equal weight. For the well-ordered parts of the surface the combination of LEED and core-level x-ray photoemission spectroscopy (XPS) favors a geometry with hydrogen adatoms bonded to the topmost carbon atoms of the first bilayer thus saturating the surface dangling bonds. However, the XPS data also show that the applied sample treatment does not yield a surface that is completely free of oxygen contamination, which must be located in the disordered parts of the surface. [S0163-1829(98)11031-7]

I. INTRODUCTION

Silicon carbide (SiC) belongs to a class of semiconductors that on account of their unique properties are suitable for high power and high-frequency applications and can be operated under extreme environmental conditions such as high temperature or high levels of radiation. The $6H$ polytype of SiC is a well suited candidate in this respect in view of its high thermal conductivity,[1] high breakdown field,[2] and electronic band gap of 3.0 eV.[3] However, there are a number of difficulties preventing the industrial application of this material. Growth of SiC material sufficiently free of defects still poses a problem that may be solved by improving the quality of the growth surfaces. The hexagonal bilayer of SiC, i.e., the (0001) plane in hexagonal and the (111) plane in cubic polytypes, is of particular importance in that respect as it is the most widely used growth plane. A number of investigations dealing with the properties of surfaces in these orientations have recently been reported whereby most of the publications[4–22] deal with qualitative aspects such as stoichiometry and surface preparation. Little experimental work, however, has been published concerning the electronic band structure of SiC. An exception with respect to the band structure of hexagonal surfaces appears to be the recent work by Johansson *et al.*[21] identifying a surface state above the valence-band maximum (VBM) on $6H$-SiC(0001), i.e., the nominally Si-terminated surface. In very recent work[23] some of the present authors determined the valence-band energies at the Γ and A critical points of the hexagonal Brillouin zone of $6H$-SiC. Otherwise, valence-band photoemission[24–27] and core-level spectroscopy measurements[28] have only been performed for β-SiC(100). Some insight into the detailed atomic structure of nominally silicon-terminated surfaces, i.e., $4H$- and $6H$-SiC(0001) and $3C$-SiC(111) came recently from low-energy electron diffraction (LEED) and scanning tunneling microscopy (STM) (Refs. 29–39) including the structure determination of the (3×3) reconstruction of $3C$-SiC(111).[40–42] On the $6H$-SiC$(000\bar{1})$ surface STM work by Hoster *et al.*[43] and a recent LEED study by some of the present authors[35,36] provided results for the atomic structure of this nominally carbon-terminated SiC surface. In this pa-

per we present results of angle-resolved photoemission measurements on the (1×1) phase of 6*H*-SiC(0001) using ultraviolet and x-ray photoelectron spectroscopy (UPS, XPS) to determine the surface-state band structure of the well-ordered parts of the surface and its chemical composition. By a detailed LEED structure analysis we present the atomic geometry of the topmost surface layers including information about the surface morphology. LEED in combination with core-level spectra from XPS provides further insight into the dangling-bond saturating adatom configuration of the well-ordered unreconstructed parts of the surface.

II. EXPERIMENT

Angle-resolved photoemission measurements were performed at the Berlin synchrotron radiation source (BESSY) using a toroidal energy analyzer[44] and a toroidal grating monochromator (TGM 4) in the photon energy range from 40 to 60 eV. The overall energy resolution was 0.25 eV and the angular resolution $\pm1°$. Angle-resolved spectra were acquired in steps of about 1° at polar angles ranging from $-90°$ to $+90°$. Angle-integrated core and valence-band spectra were also taken with a resolution of 0.5 eV using monochromatized Al $K\alpha$ x-rays (XPS, $h\nu=1486.6$ eV). The 6×6 mm^2 sample was cut from a commercial 6*H*-SiC wafer (Cree Research, Inc.), which was oriented in the [0001] direction perpendicular to the surface. After mechanical polishing, the C-terminated surface was plasma etched in a hydrogen microwave plasma (power 500 W, H_2 pressure 5×10^3 Pa, H_2 mass flow 100 sccm, sample temperature $\sim$800 °C) for about 30 min, dipped in diluted HF (5% in deionized water), and transferred into the spectrometer, which had a base pressure of 5×10^{-8} Pa. A sharp (1×1) LEED pattern with a low background was observed indicating large well ordered and unreconstructed surface parts.

A different piece of the same Cree wafer was prepared by thermal oxidation and, after a chemical cleaning procedure, removal of the oxide by means of HF and NH_4F treatment. The sample was introduced into UHV immediately after the chemical preparation using a sample transfer system. Without any further treatment this sample also exhibited a sharp (1×1) LEED pattern corresponding to the SiC-bulk periodicity. LEED measurements were carried out using a reverse view 4-grid LEED optics. The integrated diffraction spot intensities were acquired by means of a computer controlled video data acquisition system[45] resulting in intensity versus energy spectra, $I(E)$, to be compared with dynamical intensity calculations for different trial surface models (see Sec. IV).

The experimental $I(E)$ spectra can also be used as fingerprints to compare the surface structure of different samples. As described above, two different preparation methods were used in the course of these experiments. Obviously, the surface structure does not depend on the *ex situ* recipe, as can be concluded from the nearly identical $I(E)$ spectra of first-order diffraction spots shown in Fig. 1. Furthermore, we compared two different 6*H*-SiC(0001) samples, the Cree sample and a bulk grown sample that was provided by R. Helbig (Lehrstuhl für Angewandte Physik, Universität Erlangen–Nürnberg). The similarity of the intensities also shown in Fig. 1 clearly confirms the reproducibility of the preparation procedure.

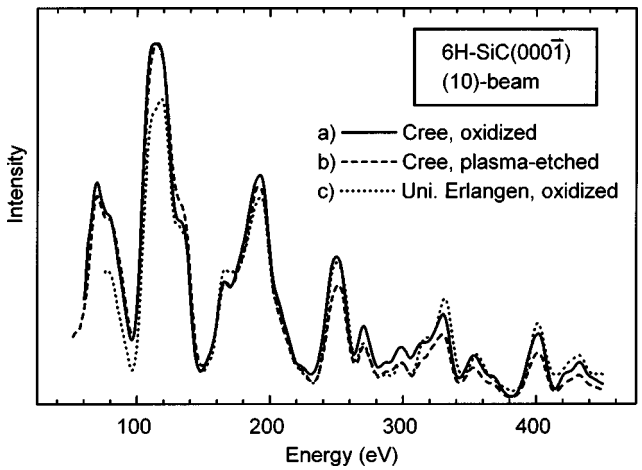

FIG. 1. LEED $I(E)$ spectra of the (10) beam from different 6*H*-SiC(0001) samples acquired immediately after HF treatment and introduction to UHV following preparation by (a) plasma etching (Cree wafer), (b) sacrificial oxidation (Cree wafer), and (c) sacrificial oxidation (Erlangen sample).

III. ELECTRONIC STRUCTURE

The angle-resolved spectra for off-normal emission were taken along the two high-symmetry azimuths $\bar{\Gamma}$-$\bar{K}$ and $\bar{\Gamma}$-$\bar{M}$ in the surface Brillouin zone (Fig. 2). $\bar{\Gamma}$-$\bar{K}$ and $\bar{\Gamma}$-$\bar{M}$ correspond to the [1210] and [1100] directions in real space, respectively. A selection of spectra for several polar angles recorded with $h\nu=52$ and 50 eV is shown in Figs. 3 and 4, respectively. The corresponding peak dispersions (binding energy vs $\mathbf{k}_{\|}$) for the two directions are displayed in Figs. 5 and 6. The magnitude of $\mathbf{k}_{\|}$ was calculated in the usual way as the projection of the photoelectron momentum onto the crystal surface. The shaded areas in Figs. 5 and 6 are the projected bulk band structures according to Ref. 46. In our previous investigation of the bulk band structure of SiC by normal emission angle-resolved photoemission spectra (ARPES),[23] we found that this band-structure calculation reproduces the experimentally determined critical point energies quite well, provided the energy scale of the calculation is stretched by 6% using the VBM as the zero of energy. The same scaling was applied in Figs. 5 and 6. It is evident that most of the experimental structures fall within the bound-

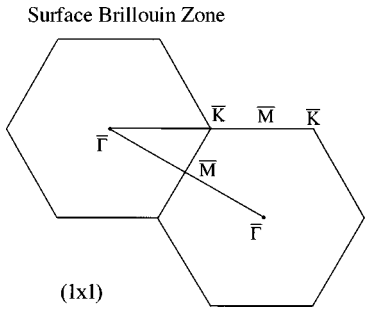

FIG. 2. Surface Brillouin zone of the (1×1) reconstructed 6*H*-SiC(0001) surface.

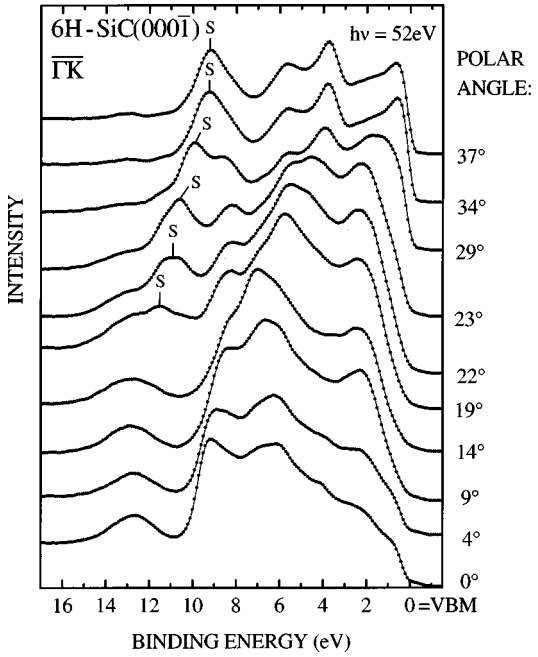

FIG. 3. Angle-resolved photoelectron spectra for several polar angles along the $\bar{\Gamma}\,\bar{K}$ azimuth of the surface Brillouin zone at a photon energy $h\nu = 52$ eV. *S* denotes emission from a surface state.

aries of the projected bulk band structure. In particular, peaks around 9 eV binding energy follow the dispersion of the boundary from $\bar{\Gamma}$ about half the way to the Brillouin zone (BZ) boundary for both azimuths with a total dispersion of more than 1 eV. Other strongly dispersing features are found around 4 eV for the $\bar{\Gamma}$-$\bar{K}$ azimuth and around 14 eV along $\bar{\Gamma}$-$\bar{M}$. Well-ordered areas on the sample surface are necessary for the observation of states dispersing with $\mathbf{k}_\parallel$; otherwise the spectra would show the dispersionless density of

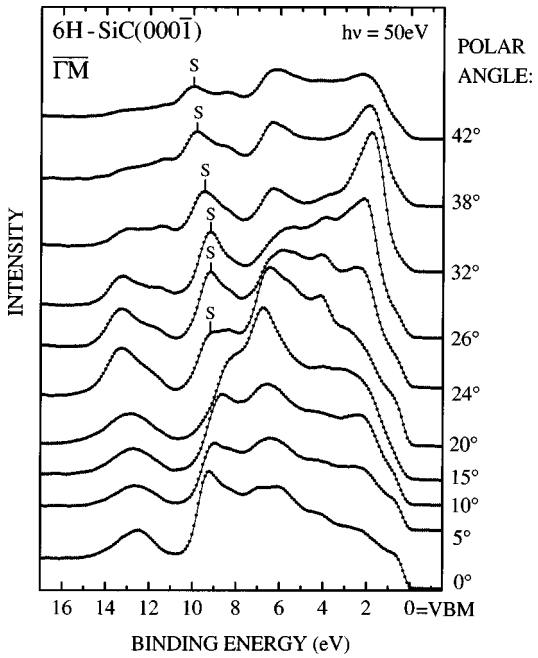

FIG. 4. Angle-resolved photoelectron spectra for several polar angles along the $\bar{\Gamma}\,\bar{M}$ azimuth of the surface Brillouin zone at a photon energy $h\nu = 50$ eV. *S* denotes emission from a surface state.

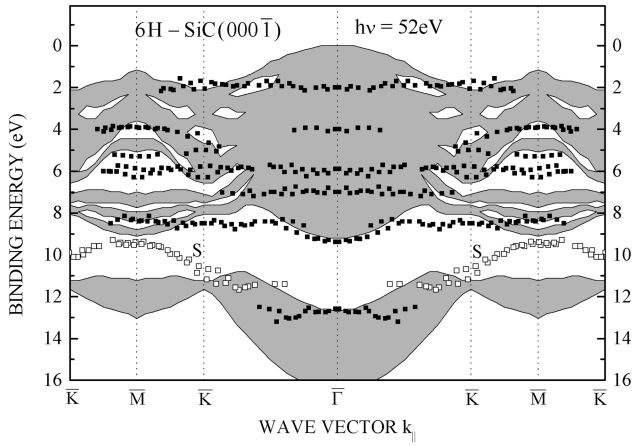

FIG. 5. Energy dispersion $E(\mathbf{k}_\parallel)$ for the azimuth $\bar{\Gamma}\,\bar{K}$ of the surface Brillouin zone as determined by angle-resolved photoelectron spectra at a photon energy $h\nu = 52$ eV. Squares denote experimentally determined states, open squares represent the surface state *S*. The shaded areas are the projected bulk band structure according to Ref. 46 after it has been stretched in energy by 6%.

states. Thus the dominance of dispersing features in the ARPE spectra indicates that only a fraction of the surface can be disordered. The nondispersing structure at about 6 eV binding energy is ascribed to emission from the O $2p$ lone pair orbital. This is due to a small amount of remaining oxygen, as will be discussed in Sec. IV.

We shall now concentrate on a strongly dispersing transition marked *S* in Figs. 3–6, which falls within the ionic gap of the bulk band structure (between 9.3 and 10.5 eV below the VBM) and must therefore be identified as emission from a surface-state band. Emission from this band can be observed as intense peaks in the spectra of both azimuths, and the dispersion fulfills all symmetry requirements such as symmetrical dispersion with respect to points $\bar{\Gamma}$ and $\bar{M}$ of the BZ, which are the center and boundary of the unreconstructed surface BZ, respectively. In order to stress the symmetry relative to the normal emission direction, which is

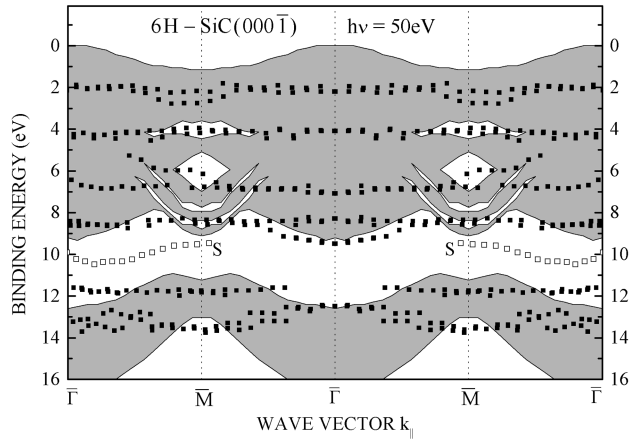

FIG. 6. Energy dispersion $E(\mathbf{k}_\parallel)$ for the azimuth $\bar{\Gamma}\,\bar{M}$ of the surface Brillouin zone as determined by angle-resolved photoelectron spectra at photon energy $h\nu = 50$ eV. Squares denote experimentally determined states, open squares represent the surface state (*S*). The shaded areas are the projected bulk band structure according to Ref. 46 after it has been stretched in energy by 6%.

represented by the central $\bar{\Gamma}$ point in Figs. 5 and 6, each feature derived from the photoelectron spectra is plotted for both positive and negative $\mathbf{k}_{\parallel}$ vectors, i.e., for positive and negative polar angles.

To our knowledge, this is the first experimental observation of electronic surface states for the 6*H*-SiC(0001) surface. Recently, Sabisch *et al.* calculated the surface-state band structure for a relaxed C-terminated 6*H*-SiC(0001) surface with carbon dangling bonds.[46] However, there are discrepancies between this calculation and our experiments. For instance, the calculation yields a surface-state band that disperses within the ionic gap between about 9.9 and 10.5 eV near the points $\bar{K}$ and $\bar{M}$ and is degenerate with bulk states around the $\bar{\Gamma}$ point. Contrary to our measurements, the binding energy for the surface state is higher at $\bar{K}$ than at $\bar{M}$. In addition, the calculation shows a rather dispersionless dangling-bond state 0.5 eV above the valence-band maximum, where we do not observe any photoelectron emission from occupied states. Accordingly, we have to assume that even those parts of the surface that exhibit the ordered (1×1) periodicity are not ideally C-terminated with unsaturated dangling bonds on the carbon atoms. In the next section we determine the geometric structure of the surface including the topmost layer stacking. In particular, we discuss whether surface dangling bonds are saturated by adatoms, which certainly would influence the energy and dispersion of any surface bands.

IV. ATOMIC SURFACE STRUCTURE

A. Surface layer stacking in 6*H*-SiC

We performed a quantitative LEED analysis to determine the surface structure of the 6*H*-SiC(0001) sample. As mentioned before, SiC is composed of tetrahedrally bonded carbon and silicon in alternating positions forming hexagonal bilayers. These bilayers are stacked on top of each other in two possible orientations, rotated by 180° with respect to each other. A single orientation of all bilayers (linear stacking) corresponds to a zinc-blende crystal structure, whereas a mutually rotated stacking of bilayers corresponds to a wurtzite structure. In SiC many different combinations of these principal stacking sequences represent stable crystal structures (see Ref. 37 for more details). The 6*H* polytype of SiC investigated here is composed of a periodic arrangement of two stacks of three linearly stacked bilayers oriented in the opposite direction (rotation by 180°). The corresponding stacking sequence is *ABCACB*... .

For a basal plane surface—which is the surface parallel to those bilayers of 6*H*-SiC—one has to distinguish between different possibilities of a *bulk truncated surface structure*. The particular layer stacking sequence of the 6*H*-polytype allows six different surface layer stacking terminations that all comply with this definition. An actual real surface may even contain a mixture of domains of different stacking sequences. The principal scenario is plotted in Fig. 7 with only three stacking sequences drawn that are distinguished by the arrangement of linearly stacked and mutually rotated bilayers (we call the different stacking arrangements *S*1, *S*2, and *S*3 according to the depth of the first orientation change). The other three possible arrangements (*S*1*, *S*2*, and *S*3*) can

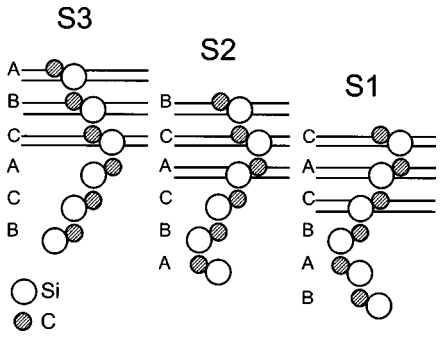

FIG. 7. Possible stacking of bilayers on a 6*H*-SiC(0001) surface shown in a cross-sectional projection parallel to the (1120) plane. The three different possible configurations are distinguished by the position of the orientation change in the bilayer stacking and labeled accordingly ($S1=CACBAB$, $S2=BCACBA$, and $S3=ABCACB$). Each termination can be present in two orientations rotated by 180° with respect to each other.

be constructed from these by a 180° rotation. They are otherwise of equivalent geometry. While any of these layer arrangements has a threefold rotational symmetry in real space, and would also show a threefold rotational symmetry in its diffraction pattern for normal primary beam incidence, the experimentally observed LEED pattern is strictly sixfold symmetric, as shown in Fig. 8. Accordingly, by symmetry arguments we conclude that a balanced ratio of *S* and *S** stacking sequences must be present on the surface.[37] Still, differently weighted surface stacking sequences (*S*1, *S*2, or *S*3) may lead to different surface-state band dispersions, which might explain the difference between the experimentally observed and theoretically predicted surface-state band energies. The domain occupation ratio is therefore one of the primary parameters to be tested in our LEED structure determination. From the absence of the dangling-bond states in the experimentally observed band structure, we might expect adatoms to be bonded to the topmost layer. The presence and nature of a dangling-bond saturation might also influence other surface states and thus could explain the difference between the measured dispersion of the surface band (*S* in

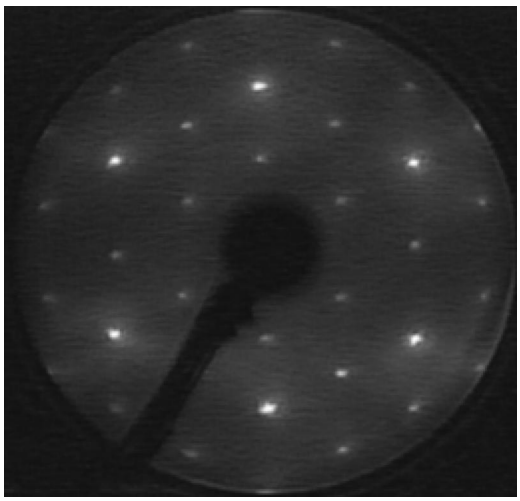

FIG. 8. LEED pattern acquired from a 6*H*-SiC(0001) surface in normal incidence geometry for 363 eV displaying sixfold rotational symmetry.

Figs. 5 and 6) and that calculated by Sabisch.[46] Accordingly, we also have to test different adatom configurations in the LEED analysis.

B. LEED intensities

Experimentally, LEED $I(E)$ spectra were acquired using a video data acquisition system as mentioned above.[45] Normal primary beam incidence was adjusted by comparing and matching the intensities of the six different spots of a single diffraction order. For five different diffraction orders of the (1×1) LEED pattern representing the (10), (11), (20), (21), and the (30) spot all symmetry equivalent spectra were then acquired and averaged. For trial surface models, LEED intensities were generated using full dynamical calculations based on standard computer programs.[50,51] The atomic scattering properties were modeled using 11 relativistically calculated and spin-averaged phase shifts based on potentials obtained from a bulk SiC crystal. Electron attenuation was simulated by the imaginary part of the optical potential V_{0i}, which was considered energy dependent according to $V_{0i}\sim E^{1/3}$.[52] The actual magnitudes of V_{0i} were adapted from our previous analysis of $6H$-SiC(0001) (Ref. 29) and correspond to $V_{0i}=4$ eV for the clean surface and $V_{0i}=3.5$ eV for the adatom models at a primary energy of 90 eV. Thermal vibrations were considered within the Debye model. Vibration amplitudes were also taken from a previous analysis[35] and for both surface and bulk equivalent to Debye temperatures of $\Theta_D=750$ K for silicon and $\Theta_D=860$ K for carbon. Adatom vibration amplitudes were set to the same value as for the topmost carbon atoms. The real part of the inner potential V_{0R} was fitted as usual by shifting experimental and theoretical intensities on the energy scale. Bilayers had to be treated as composite layers using the combined space method[51,53] due to their small thickness (0.63 Å in the bulk). Scattering between bilayers was considered using the layer doubling scheme.[50,54] Submonolayer coverages in the adatom layers were tested by using the average t-matrix approximation (ATA) where the scattering amplitudes of two elements, or here the element and a vacancy, are averaged according to the atomic concentration.[55] The intensities were calculated for energies up to 400 eV. As the different beams appear on the fluorescent screen at different energies—the (30) spectrum starts only at 370 eV—this amounts to a total energy overlap between experiment and theory of 835 eV. By optimizing the agreement between experimental and theoretical intensity spectra, which was quantified by the Pendry R factor R_p,[56] the correct model was determined. Using a statistical error estimate based on the variance of R_p, we could judge the significance of a fit improvement.[56] It was necessary to employ an automated search algorithm[57] in order to be able to scan through the large parameter space, which would otherwise be practically impossible to handle.

C. LEED structure analysis

Among the models considered were all three different surface stacking sequences alone and combined in different mixing ratios. In all cases the sixfold symmetric LEED pattern was generated by averaging the intensities calculated for equally weighted S and S^* domains of identical geometry. For each individual domain type several interlayer spacing parameters were varied, including the topmost bilayer thickness (d_{11}) and up to three spacings between bilayers [D_{ij}, see Fig. 9(a)]. Finally, hydrogen, oxygen, and silicon adatoms were included in the model variation in different high-symmetry bonding geometries, accounting for a possible saturation of dangling bonds. We tested the $T1$ site where the adatom is located on top of the topmost carbon atom and two threefold hollow sites, one with the adatoms above a Si atom in the topmost bilayer, i.e., quasi-fourfold-coordinated ($T4$ site), and one with the adatoms above the second bilayer Si position, i.e., truly threefold coordinated ($H3$ site).[29] Note that a model with silicon in $T1$ geometry simulates a half-bilayer although this appears to be an energetically unfavorable structure. Full and submonolayer concentrations were tested for oxygen and hydrogen. In addition, two oxide type models were tried, one with linear Si-O species oriented along the surface normal direction and bonded to the topmost carbon atoms of the first bilayer, and the other with a Si-O bilayer linearly stacked on top of the topmost substrate SiC bilayer. For clarity, the different adatom models are plotted in Fig. 9 [panels (b)–(d)]. In these models the same substrate interlayer spacings were varied as in the clean surface model [panel (a)]. In addition, the spacing between the topmost substrate and the adatom layer (d_{01}), and in the case of the Si-O models [panels (c) and (d)] the vertical spacing between Si and O, (d_{-10}), were considered.

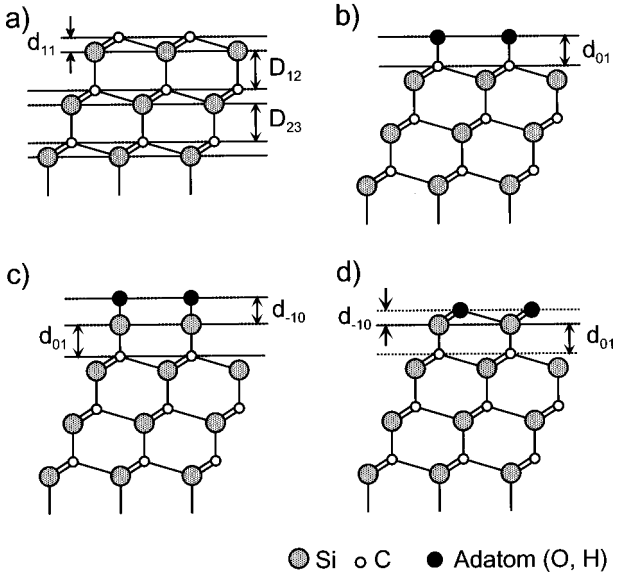

FIG. 9. The SiC(000$\bar{1}$) surface models tested in the LEED analysis: (a) A clean unreconstructed surface terminated by a full bilayer. The topmost bilayer thickness (d_{11}) and the first two interbilayer spacings (D_{ij}) are given. (b) Adatom model with adatoms in $T1$ coordination. $H3$ and $T4$ sites were also tested. The bond length (d_{01}) is shown in the plot. (c) Surface normal, linear Si-O species in $T1$ position. C-Si (d_{01}) and Si-O (d_{-10}) bond lengths are indicated. (d) Si-O bilayer linearly continuing the substrate stacking sequence. Here d_{01} is the C-Si bond length and d_{-10} the Si-O bilayer thickness.

In a first step of the analysis the substrate geometry was tested without adatoms. An almost equally weighted mixture of all three possible stacking sequences yielded an R factor of $R_p=0.198$. The dominance of a single domain type as found previously on a $6H$-SiC(0001) surface[29] could be ex-

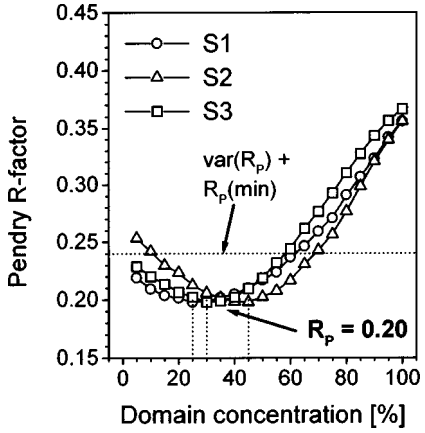

FIG. 10. *R*-factor plots for different mixtures of *S*1, *S*2, and *S*3 type domains (discussed in the text).

cluded with *R* factors not lower than 0.35. The exact domain-type ratios can be deduced from the *R*-factor analysis as shown in Fig. 10 and were found to be 25% (*S*1/*S*1*), 30% (*S*2/*S*2*), and 45% (*S*3/*S*3*). However, the deviation from a 1:1:1 mixture is not statistically significant as judged by the variance of the *R* factor (0.04, cf. Fig. 10). Using the variance level of the *R* factor we can estimate the error margin for the mixing ratios to be about ±20%. It should be noted that the *R*-factor curves shown for the domain mixture are obtained by fixing the percentage value of *one* domain and optimizing all other geometrical and percentage parameters of the surface model avoiding cross correlations and so yielding the true statistical error in the multidimensional parameter space. Bilayer spacings as derived from the best fit are more or less bulklike (1.89 Å) below the surface while the first bilayer is on average compressed by 20% (see Table I for exact values). When no adatoms are considered in the fit (clean surface in Table I), the trends for layer spacing relaxations qualitatively agree with the structure optimized by total energy calculations.[46,58] There, the topmost bilayer is compressed even more to 0.38 Å (compared to a domain average of 0.51 Å from LEED) while the first bilayer distance is expanded to 1.97 Å (1.90 Å from LEED). The balanced presence of all three possible domain types compares well to the observation by transmission electron microscopy of equally distributed single bilayer height steps on the (0001) orientation of as-grown homoepitaxial 4*H*- and 6*H*-SiC layers.[59] Such a configuration requires a 1:1:1 mixture of domains. We therefore assume that a single step morphology is present on our 6*H*-SiC$(000\bar{1})$ sample as well.

The picture of a domain mixture does not change dramatically when adatoms are included in a refinement analysis. For some models the percentage numbers slightly change, but never significantly enough to exclude an equally weighted mixture. In fact, for none of the adatom models does the *R* factor decrease to an extent that the clean surface as described above would be outside the error limits. For a full monolayer oxygen coverage, the *R* factor even rises. The Si-O bilayer model yields the same R_p value as the clean surface, which probably is just an indication that the scattering properties of oxygen and carbon are rather similar, at least for non-forward-scattering angles. However, even for a planar layer the Si-O bond length (1.78 Å) would be too large. Hence, this model seems improbable. No minimum of the *R* factor appears for any geometry of the linear Si-O model, thus it also has to be excluded. Only for a hydrogen layer or submonolayer concentrations of oxygen both in *T*1 position, i.e., sitting on top of the topmost carbon atom, can the fit be improved. With 100% hydrogen covering all three domains with an average bond length of $d_{01}=1.02$ Å, the *R* factor drops to $R_p=0.184$. The best fit for oxygen is even lower with $R_p=0.168$, however still not outside the *R*-factor variance. In the case of partial oxygen termination, the optimum oxygen coverage is found to be 26% with a bond length $d_{01}=1.40$ Å as averaged over the three domains. In both cases (hydrogen and oxygen) the bond lengths are in a reasonable range and compare very well to 1.10 Å in molecular C-H bonds and 1.43 Å in σ bonded C-O. In Table I the best-fit geometries and the resulting *R* factors are summarized for the adatom model search. In addition, the bulk layer spacings and the optimized structure of the total energy calculations[46] are given. Nevertheless, from the LEED analysis alone we cannot determine a best-fit adatom model that is significantly better than the clean surface itself. However, as discussed in the next paragraph, evidence from XPS allows us to favor one of the models.

TABLE I. Best values of domain mixing percentages, layer spacing, adatom coverage, and *R* factor for the different surface models considered. Individual values for each domain and an average evaluated according to the mixing ratio is given. In addition, layer stacking values are given for the SiC bulk and for the surface structure optimized by total energy calculations (Ref. 46). A dash is listed when the respective parameter was not varied in the calculation.

Model	Clean surface				Hydrogen adatoms				Oxygen adatoms				SiO layer				Bulk	Ref. 46
Domain	*S*3	*S*2	*S*1	av	*S*3	*S*2	*S*1	av	*S*3	*S*2	*S*1	av	*S*3	*S*2	*S*1	av		
mix (%)	45	30	25		30	45	25		30	45	25		45	30	25			
d_{11} (Å)	0.53	0.53	0.47	0.51	0.57	0.63	0.60	0.60	0.57	0.54	0.63	0.57	-	-	-	-	0.63	0.38
D_{12} (Å)	1.89	1.91	1.89	1.90	1.94	1.94	1.84	1.91	1.94	1.94	1.79	1.90	1.84	1.94	1.89	1.88	1.89	1.88
D_{23} (Å)	1.83	1.89	1.91	1.87	1.89	1.89	1.84	1.88	1.89	1.89	1.84	1.88	1.94	1.84	1.89	1.90	1.89	1.88
D_{34} (Å)	1.95	1.92	1.92	1.93	-	-		-		-		-		-		-	1.89	-
d_{01} (Å)	-	-	-	-	1.03	1.03	1.00	1.02	1.38	1.38	1.44	1.40	1.84	1.89	1.89	1.87		
d_{-10} (Å)	-	-	-	-	-	-	-	-	-	-	-	-	0.25	0.25	0.44	0.30		
ad(%)	-	-	-	-	100	100	100	100	30	20	30	26	100	100	100	100		
R_P	0.198				0.184				0.168				0.178					

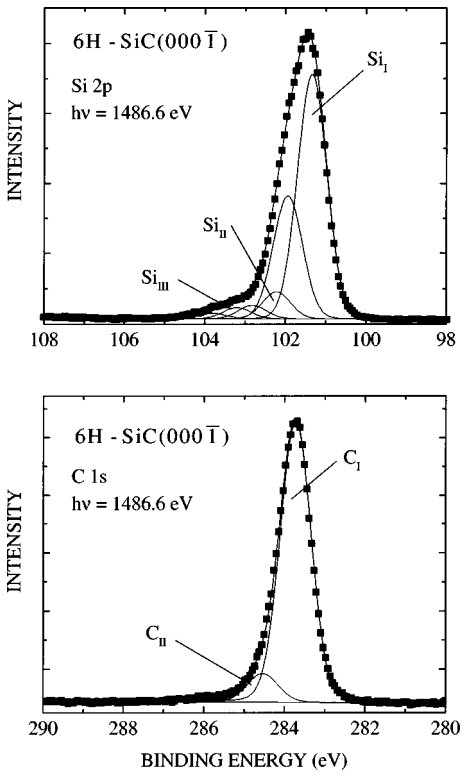

FIG. 11. Si $2p$ and C $1s$ XPS core-level spectra of $6H$-SiC(0001). The meaning of the labels Si_I, Si_{II}, etc. is explained in the text.

D. Additional structural information from XPS

In XPS we observe a single, slightly asymmetric C $1s$ line at a binding energy of 283.7 eV and a Si $2p$ line at 101.3 eV (Si_I) with a minute shoulder at 103.8 eV (see Fig. 11). The shoulder on the Si $2p$ spectrum can be fitted by two chemically shifted components located at 102.2 eV (Si_{II}) and 103.2 eV (Si_{III}). The sum of Si_{II} and Si_{III} amounts to about 13% of the total Si $2p$ intensity. On account of an O $1s$ signal at 533.0 eV these shifted Si components can be ascribed to silicon suboxides. However, according to the LEED analysis as discussed above, oxygen bonded to Si can be ruled out. Therefore, this oxide cannot be present on the well-ordered parts of the surface but rather seems to reside in scratches that remained from the mechanical polishing and could not be removed in the course of the surface preparation. In fact, the amount of oxide as judged from the oxygen signal corresponds approximately to the equivalent of one monolayer while the shifted silicon signal can only account for about half of it. The C $1s$ core-level spectrum of the $6H$-SiC(0001) surface shown at the bottom of Fig. 11 can be fitted with the major component at 283.7 eV (C_I) and a minor one shifted by 0.8 eV (C_{II}) towards higher binding energies, which amounts to ~9% of the total C $1s$ intensity. A conspicuous absence of C $1s$ components shifted by 3–6 eV towards higher binding energies precludes a measurable amount of oxygen bonded to carbon.[48,49] That also confirms that there is no oxygen within the well-ordered, carbon-terminated parts of the surface. Accordingly, we have to dismiss the oxygen adatom model in $T1$ geometry although it yields overall the best R factor in the LEED analysis.

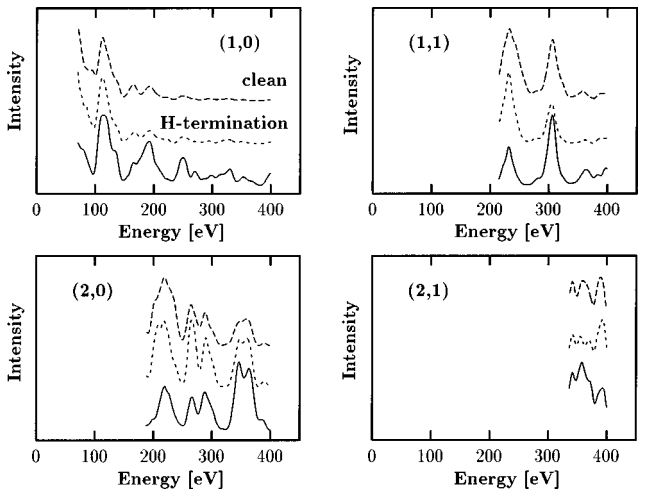

FIG. 12. Comparison of experimental (solid lines) and calculated LEED spectra for the favored hydrogen adatom model (short dashed lines) and the optimized geometry for a clean surface (long dashed lines).

We noted above that the theoretical calculations by Sabisch *et al.* predict a dangling-bond surface state about 0.5 eV above the valence-band maximum on a relaxed, C-terminated $6H$-SiC(0001) surface with carbon dangling bonds.[46] However, in the valence-band spectra discussed in Sec. III, no indication for the existence of such a valence band is observed. Thus, the clean surface as tested in the LEED analysis is also incompatible with the spectroscopic evidence. Only the model with hydrogen termination ($R_p = 0.184$) is thus consistent with all data sets. It is not possible to identify the nature of the shifted C $1s$ component unambiguously. It might be attributed to a graphitic impurity related to the disordered parts of the surface, or to a small chemical shift due to a hydrogen bond in the well-ordered parts. A similar shoulder was indeed observed for a hydrogen exposed diamond (111) surface.[47] Thus, from the combination of LEED and XPS we conclude for the well-ordered parts of our sample surface that the only possible species of adatoms saturating the surface dangling bonds is hydrogen. Unfortunately, theoretical calculations including adatoms in the (1×1) structure have not been published to our knowledge. The LEED spectra for the best-fit hydrogen model and the clean surface alone are shown in Fig. 12 in comparison to the experimental data [the (30) beam is omitted in view of its small energy range]. The visual agreement between experiment and theory is very good for both geometry models. The R-factor improvement for the hydrogen model primarily results from the better reproduction of the first peak in the (11) beam. Nevertheless, the overall scattering cross section for hydrogen is too small to cause significant differences in the LEED intensities, as is well known and manifested in the small absolute R-factor improvement.

V. SUMMARY

We succeeded in preparing $6H$-SiC(000$\bar{1}$) surfaces with large, well-ordered, and unreconstructed areas by either a hydrogen plasma treatment in a microwave discharge and subsequent HF treatment or by growing a sacrificial oxide

and subsequent HF treatment. The equivalent of one monolayer oxygen is located in scratches that are left over after mechanical polishing and therefore does not interfere with band dispersions measured in angle-resolved photoemission and with the analysis of LEED $I(E)$ spectra. In ARPES a dispersing bulk and a strongly dispersing surface state in the ionic gap but no dangling-bond state above the VBM are observed. The origin of this surface electronic structure has not been identified by calculations so far.

In the quantitative LEED structure determination we obtained a best fit for a model for the well-ordered parts of the surface containing a nearly equally weighted mixture of domains with different stacking sequences of the topmost bilayers. The fit is improved by hydrogen and oxygen adatoms in $T1$ position, not to an extent, however, to exclude the clean surface model. Yet, in combination with evidence from the core-level spectra and in absence of a dangling-bond state, we favor the hydrogen model rather than a clean surface and exclude oxygen adatoms. Nevertheless it should remain clear that concluding the presence of hydrogen is based on indirect evidence. We have not been able to directly observe hydrogen on the surface.

ACKNOWLEDGMENTS

This work was supported by the Deutsche Forschungsgemeinschaft through SFB 292 and the Bundesministerium für Bildung, Forschung, Wissenschaft und Technologie, Contract No. 05622WEA7. U.S. acknowledges additional support by the DFG through Grant No. STA315/4. We would like to thank the staff of BESSY, especially Walter Braun, for their help during the experiments, and Magdalena Sabisch for providing her band-structure calculations prior to publication. We also acknowledge the help of Reinhard Stöckel and Klemens Janischowsky, who performed the hydrogen plasma preparation.

[1] E. A. Burgemeister, W. von Münch, and E. Pettenpaul, J. Appl. Phys. **50**, 5790 (1979).
[2] B. J. Baliga, Springer Proc. Phys. **71**, 305 (1992).
[3] W. Choyke, D. R. Hamilton, and L. Patrick, Phys. Rev. **133**, A1163 (1964).
[4] J. A. Dillon, Jr., R. E. Schlier, and H. E. Farnsworth, J. Appl. Phys. **30**, 675 (1959).
[5] A. J. van Bommel, J. E. Crombeen, and A. van Tooren, Surf. Sci. **48**, 463 (1975).
[6] F. Bozso, L. Muehlhoff, M. Trenary, W. J. Choyke, and J. T. Yates, Jr., J. Vac. Sci. Technol. A **2**, 1271 (1984).
[7] S. Adachi, M. Mohri, and T. Yamashina, Surf. Sci. **161**, 479 (1985).
[8] L. Muehlhoff, W. J. Choyke, M. J. Bozack, and J. T. Yates, J. Appl. Phys. **60**, 2842 (1986).
[9] R. Kaplan and T. M. Parrill, Surf. Sci. Lett. **165**, L45 (1986).
[10] R. Kaplan, Surf. Sci. **215**, 111 (1989).
[11] S. Nakanishi, H. Tokutaka, S. Nishimori, S. Kishida, and N. Ishihara, Appl. Surf. Sci. **41/42**, 44 (1989).
[12] C.-S. Chang, I. S. T. Tsong, Y. C. Wang, and R. F. Davis, Surf. Sci. **256**, 354 (1991).
[13] M.-H. Tsai, C. S. Chang, J. D. Dow, and I. S. T. Tsong, Phys. Rev. B **45**, 1327 (1992).
[14] M. A. Kulakov, P. Heuell, V. F. Tsetkov, and B. Bullemer, Surf. Sci. **315**, 248 (1994).
[15] V. M. Bermudez, Appl. Surf. Sci. **84**, 45 (1995).
[16] Y. Marumoto, T. Tsukamoto, M. Hirai, M. Kusaka, M. Iwami, T. Ozawa, T. Nagamura, and T. Nakata, Jpn. J. Appl. Phys., Part 1 **34**, 3351 (1995).
[17] H. Nienhaus, T. U. Kampen, and W. Mönch, Surf. Sci. Lett. **324**, L328 (1995).
[18] L. I. Johansson, F. Owman, and P. Mårtensson, Surf. Sci. Lett. **360**, L483 (1996).
[19] L. I. Johansson, F. Owman, P. Mårtensson, C. Persson, and U. Lindefelt, Phys. Rev. B **53**, 13 803 (1996).
[20] L. I. Johansson, F. Owman, and P. Mårtensson, Phys. Rev. B **53**, 13 793 (1996).
[21] L. I. Johansson, F. Owman, and P. Mårtensson, Surf. Sci. Lett. **360**, L478 (1996).
[22] L. Li, C. Tindall, O. Takaoka, Y. Hasegawa, and T. Sakurai, Surf. Sci. **385**, 60 (1997).
[23] M. Hollering, A. Ziegler, R. Graupner, B. Mattern, L. Ley, A. P. J. Stampfl, J. D. Riley, and R. C. G. Leckey, Diamond Relat. Mater. **6**, 1358 (1997).
[24] T. M. Parrill and V. M. Bermudez, Solid State Commun. **63**, 231 (1987).
[25] V. M. Bermudez, J. Appl. Phys. **66**, 6084 (1989).
[26] V. Yu. Aristov, L. Douillard, O. Fauchoux, and P. Soukiassian, Phys. Rev. Lett. **79**, 3700 (1997).
[27] P. Käckell, F. Bechstedt, H. Hüsken, B. Schröter, and W. Richter, Surf. Sci. Lett. **391**, L1183 (1997).
[28] J. P. Long, V. M. Bermudez, and D. E. Ramaker, Phys. Rev. Lett. **76**, 991 (1996).
[29] J. Schardt, C. Bram, S. Müller, U. Starke, K. Heinz, and K. Müller, Surf. Sci. **337**, 232 (1995).
[30] U. Starke, C. Bram, P.-R. Steiner, W. Hartner, L. Hammer, K. Heinz, and K. Müller, Appl. Surf. Sci. **89**, 175 (1995).
[31] U. Starke, J. Schardt, P.-R. Steiner, W. Hartner, S. Müller, L. Hammer, K. Heinz, and K. Müller, in *Proceedings: Symposium on Surface Science 3S'95* (Inst. f. Allg. Physik, TU Wien, Wien, 1995), p. 11.
[32] F. Owman and P. Mårtensson, Surf. Sci. Lett. **330**, L639 (1995).
[33] M. A. Kulakov, G. Henn, and B. Bullemer, Surf. Sci. **346**, 49 (1996).
[34] L. Li and I. S. T. Tsong, Surf. Sci. **351**, 141 (1996).
[35] J. Schardt, J. Bernhardt, U. Starke, and K. Heinz, Surf. Rev. Lett. **5**, 181 (1998).
[36] U. Starke, J. Bernhardt, M. Franke, J. Schardt, and K. Heinz, Diamond Relat. Mater. **6**, 1349 (1997).
[37] U. Starke, Phys. Status Solidi B **202**, 475 (1997).
[38] U. Starke, J. Schardt, and M. Franke, Appl. Phys. A: Mater. Sci. Process. **65A**, 587 (1997).
[39] J. Schardt, J. Bernhardt, M. Franke, U. Starke, and K. Heinz, Mater. Sci. Forum **264-268**, 343 (1998).
[40] K. Reuter, J. Bernhardt, H. Wedler, J. Schardt, U. Starke, and K. Heinz, Phys. Rev. Lett. **79**, 4818 (1997).
[41] U. Starke, J. Schardt, J. Bernhardt, M. Franke, K. Reuter, H. Wedler, K. Heinz, J. Furthmüller, P. Käckell, and F. Bechstedt,

Phys. Rev. Lett. **80**, 758 (1998).
[42] U. Starke, M. Franke, J. Bernhardt, J. Schardt, K. Reuter, and K. Heinz, Mater. Sci. Forum **264-268**, 321 (1998).
[43] H. E. Hoster, M. A. Kulakov, and B. Bullemer, Surf. Sci. Lett. **382**, L658 (1997).
[44] R. C. G. Leckey and J. D. Riley, Appl. Surf. Sci. **22/23**, 196 (1985).
[45] K. Heinz, Rep. Prog. Phys. **58**, 637 (1995).
[46] M. Sabisch, P. Krüger, and J. Pollmann, Phys. Rev. B **55**, 10 561 (1997).
[47] R. Graupner, J. Ristein, and L. Ley, Surf. Sci. **320**, 201 (1994).
[48] A. T. S. Wee, Z. C. Feng, H. H. Hng, K. L. Tan, C. C. Tin, R. Hu, and R. Coston, Appl. Surf. Sci. **81**, 377 (1994).
[49] G. Beamson and D. Briggs, *High Resolution XPS of Organic Polymers* (Wiley, Chichester, 1992).
[50] J. B. Pendry, *Low Energy Electron Diffraction* (Academic, London, 1974).
[51] M. A. Van Hove and S. Y. Tong, *Surface Crystallography by LEED* (Springer, Berlin, 1979).
[52] J. E. Demuth, P. M. Marcus, and D. W. Jepsen, Phys. Rev. B **11**, 1460 (1975).
[53] S. Y. Tong and M. A. Van Hove, Phys. Rev. B **16**, 1459 (1977).
[54] M. A. Van Hove and J. B. Pendry, J. Phys. C **8**, 1362 (1975).
[55] Y. Gauthier, Y. Joly, R. Boudoing, and J. Rundgren, Phys. Rev. B **31**, 6216 (1985).
[56] J. B. Pendry, J. Phys. C **13**, 937 (1980).
[57] M. Kottcke and K. Heinz, Surf. Sci. **376**, 352 (1997).
[58] M. Sabisch, P. Krüger, A. Mazur, and J. Pollmann, Surf. Rev. Lett. **5**, 199 (1998).
[59] T. Kimoto, A. Itoh, H. Matsunami, and T. Okano, J. Appl. Phys. **81**, 3494 (1997).